Journal of Applied Electrochemistry **30**: 809–816, 2000.

A new technique for the visualization of the concentration boundary layer in an electrodialysis cell

V. PÉREZ-HERRANZ*, J.L. GUIÑÓN and J. GARCÍA-ANTÓN
Departamento de Ingeniería Química y Nuclear, E.T.S.I. Industriales. Universidad Politécnica de Valencia, PO Box. 22012, 46071 Valencia, Spain
*(*author for correspondence)*

Received 7 June 1999; accepted in revised form 22 February 2000

Key words: concentration boundary layer, electrodialysis, flow visualization

Abstract

A new method for the visualization of the concentration boundary layer is described. The technique involves the use of a dilute solution of an indicator which reacts with H^+ formed on the membrane surface to form a coloured trace when the electrodialysis cell is operating above the limiting current density. The thickness of the concentration boundary layer determined by the visualization method agrees well with results obtained from limiting current density measurements and theoretical predictions. The visualization method proposed in this work can be used for understanding the transport taking place between a solid wall and a liquid in steady and unsteady flow processes.

List of symbols

a pulsation amplitude (m)
C_∞ concentration (mol m^{-3})
D diffusion coefficient ($m^2\,s^{-1}$)
F Faraday constant ($C\,mol^{-1}$)
I current (A)
i_{lim} limiting current density ($A\,m^{-2}$)
Re_x longitudinal Reynolds number ($u\,x/v$)
S membrane exchange area (m^2)
Sc Schmidt number (v/D)
T pulsation period (s)
t time (s)
$\bar{t}_j$ transference number in the membrane
t_j transference number in the solution
x distance from the entrance of the liquid to the cell (m)
X dimensionless distance
x_0 distance at which the membrane is situated (m)
U cell voltage (V)
u fluid velocity ($m\,s^{-1}$)
z_j electrical charge of ions

Greek letters
δ_1 thickness of the hydrodynamic boundary layer (m)
δ thickness of the concentration boundary layer (m)
v kinematic viscosity ($m^2\,s^{-1}$)
ρ density ($kg\,m^{-3}$)
ω pulsation frequency (s^{-1})

1. Introduction

Among the techniques used to study the shape and thickness of the boundary layer in laminar and turbulent flows, hot wire anemometry, Laser Doppler velocimetry, measurements of wall shear magnitude and direction using oil-flow methods, photographic and holographic interferometry, pulse luminescence, photochromic tracer techniques, or visualization techniques based on metals electrodeposition are described in references [1–8]. However, some of these techniques, based on dye injection, and other techniques such as wires used to generate hydrogen bubbles, widely used to study the hydrodynamic and thermal boundary layers, can influence events in the sensitive region of the boundary layer by creating disturbances.

In the case of electrodialysis systems, the concentration boundary layer has been determined using different techniques. Sanchez and Clifton [9], and Shaposhnik et al. [10] used interferometric techniques for the visualization of the concentration gradient on the membrane surface. Then the thickness of the concentration boundary layer is calculated from the concentration gradient. Other techniques used for the determination of the thickness of the concentration boundary layer are based on self-diffusion measurements of labelled ions [11], measurements of the limiting current density [12], estimation of the concentration gradient from measurements of back electromotive force [13] or from chronopotentiometric studies [14].

In this work, an experimental study of the phenomena occurring near the wall region and the thickness of the concentration boundary layer in an annular electrodialysis cell are examined using a new tracer technique using a chemical indicator for flow visualization in laminar steady and pulsating flow. The technique used is

nondisturbing, since the tracer is not required to be inserted into the flow, it shows the flow clearly, can be accurate and can be related directly to mass transfer. Photographic results and a discussion of data are given and compared with the results of the thickness of the concentration boundary layer obtained from the measurement of the limiting current density and from the theoretical predictions. The present data also serve for the study and understanding of the physical phenomena that take place on the surface of an ionic exchange membrane in an electrodialysis cell when operating at current densities higher than the limiting current density.

2. Experimental details

The experimental arrangement used is shown in Figure 1. The annular electrodialysis cell consisted of a 300 mm high Plexiglas column with an inner diameter of 80 mm. The inner cylinder of the annular cell consisted of a 300 mm high PVC framework, with a 40 mm outer diameter in which the anionic membrane was supported. The framework-membrane assembly separated the cell into two concentric cylinders. The outer cylinder, which acted as the cathodic dilution compartment, is where concentration polarization takes place, and the concentration boundary layer is visualized. The inner cylinder acted as anodic compartment, or concentration compartment. A scheme of the electrodialysis cell configuration is shown in Figure 2.

The membrane used in this work was an anionic membrane type 204-SXZL-386 (IONICS) and was situated 100 mm above the access of the fluid to the cell. The membrane length was 50 mm. The exchange area of the membrane was, $S = 6.28 \times 10^{-3}\,m^2$.

A solution of 0.1 M NaCl was chosen as the electrolyte and 10^{-5} M methyl red was used as the analytical indicator. Before use, the membrane was soaked in a NaCl solution of the same concentration

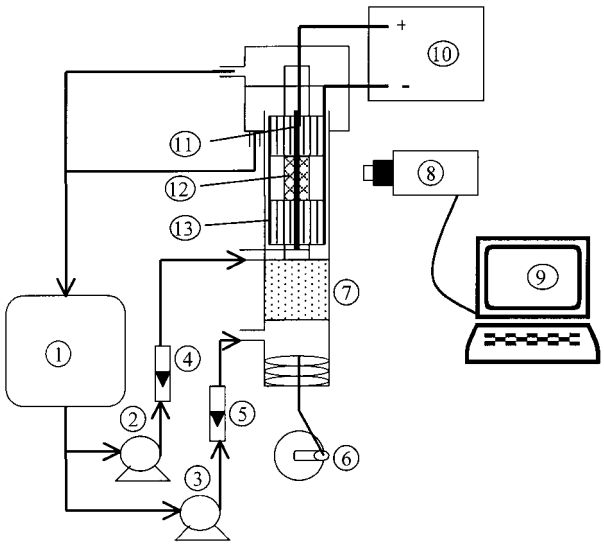

Fig. 1. Scheme of the experimental arrangement: (1) storage tank, (2) and (3) pumps, (4) and (5) rotameters, (6) pulsation system, (7) calming section, (8) video camera, (9) computer, (10) power supply, (11) anode, (12) membrane and (13) cathode.

for 24 h. The physical properties of the electrolyte at 25 °C were: density, $\rho = 1002.4\,kg\,m^{-3}$, kinematic viscosity, $\nu = 1.0106 \times 10^{-6}\,m^2\,s^{-1}$, diffusion coefficient of NaCl obtained from [15], $D = 1.483 \times 10^{-9}\,m^2\,s^{-1}$. The transport number of chloride ions in the solution, calculated from the values of the ionic mobilities of sodium and chloride ions at infinite dilution was $t_{Cl^-} = 0.6$, while the transport number for chloride ions across the membrane in a 0.1 M NaCl solution was $t_{Cl^-} = 0.96$.

The cathode was a 70 mm diameter and 100 mm high AISI 316 stainless steel cylindrical grid. The anode was a 200 mm high lead–antimony (10% Sb) bar.

Beneath the cell, was a 150 mm long calming section filled with 3 mm diameter glass spheres. The main purpose of this section was to prevent channelling and to ensure a uniform flow distribution at the entrance of

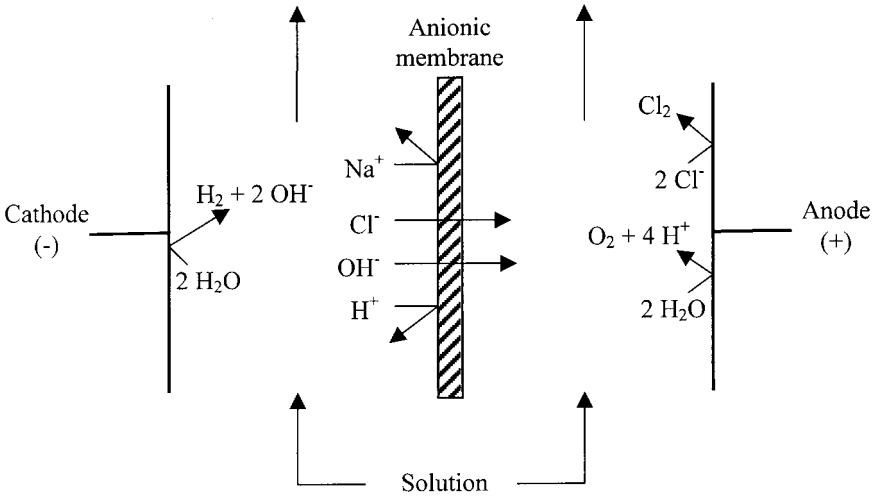

Fig. 2. Scheme of the electrodialysis cell configuration.

the cell. The calming section was separated from the cell by a grid to prevent any fluidization phenomena of the bed.

To study the effect of pulsating flow on the concentration boundary layer, the solution passing through the dilution compartment was linked to a piston driven by an electric motor. Further details of the pulsation system can be found in [16].

The thickness of the concentration boundary layer was determined from the video image analysis. The video camera was connected to a frame-grabber board which was implemented in a PC. The board digitized the images received by the camera into an array of 320×240 pixels of 24 bits at 15 frames per second. The pictures were stored on the hard disc of the computer and further processed.

The operating current density for the visualization experiments was twice the limiting current density, as it was found from other experiments that if the applied current is sufficiently high, the coloured area corresponding to the concentration boundary layer is independent of the applied current.

3. Background

Electrodialysis is an electrochemical separation process in which ions are transferred through permselective membranes under the influence of an electric field. When the applied current density in an electrodialysis process exceeds the limiting current density, water splitting can take place. Then, H^+ ions are transferred through cationic membranes and OH^- ions are transferred through anionic membranes, leading to pH changes in the boundary layers close to the membrane. Apart from pH changes, working at current densities above the limiting current density in an electrodialysis process causes problems such as scale formation, membrane breakage and an increase in electrical energy consumption [17–18]. Based on Nernst–Plank equation, the limiting current density can be evaluated using the following expression:

$$i_{\lim} = \frac{z_j F D C_\infty}{\delta(\bar{t}_j - t_j)} \tag{1}$$

where $i_{\lim}$ is the limiting current density, z_j the electrical charge of the ion to be transferred, D the diffusion coefficient of the electrolyte, F the Faraday constant, C_∞, the bulk solution concentration, δ the thickness of the concentration boundary layer, and $\bar{t}_j$ and t_j are the transference numbers of the ion in the membrane and in the solution, respectively.

The limiting current density is one of the most important design parameters in electrodialysis, and its value must not be exceeded. As can be concluded from Equation 1, the limiting current density depends on the thickness of the concentration boundary layer, and therefore, the fluid velocity exerts a major influence on the limiting current density.

The thickness of the concentration boundary layer, δ, formed on a flat surface in laminar flow can be estimated from the following expression [19]:

$$\delta = 4.64\, x Re_x^{-1/2} \left(\frac{Sc}{X}\right)^{-1/3} \tag{2}$$

where x is the distance from the entrance of the fluid to the electrodialysis cell, Re_x is the longitudinal Reynolds number, $Re_x = u x/v$, Sc is the Schmidt number, $Sc = v/D$, and X is a dimensionless distance defined by the following equation:

$$X = 1 - \left(\frac{x_0}{x}\right)^{3/4} \tag{3}$$

where x_0 represents the point where the membrane is situated and the concentration boundary layer is formed.

Equation 2 represents Karman's approximate model for the thickness of the concentration boundary layer, and can be applied for high Schmidt numbers, when the thickness of the hydrodynamic boundary layer is higher than that of the concentration boundary layer.

The technique used in this work for the visualization of the concentration boundary layer is based on the pH change occurring on the membrane surface of the dilution compartment, as a consequence of water splitting, when the limiting current density is exceeded. This technique is similar to the electrode activated pH method used for flow visualization [20, 21]. However, in the electrode activated pH method, the pH change is due to the anodic hydroxyl ion oxidation or cathodic hydroxyl ion reduction on the electrode surface, while in the technique used in this work, the pH change is due to the water splitting which takes place on the membrane surface in the dilution compartment.

As a consequence of water splitting, hydroxyl ions are transferred to the concentration compartment across the anionic membrane, while protons remain in the dilution compartment close to the membrane surface. Then a gradient in the proton concentration is created between the membrane surface and the bulk solution, located in the concentration boundary layer. This situation generates a pH difference between the concentration boundary layer and the solution. If a suitable analytical indicator is used, the pH difference between the concentration boundary layer and the solution produces a change in the colour of the indicator in both zones. An appropriate indicator is the methyl red, whose colour changes in the pH interval ranging between 4.4 and 6.2. Thus the solution with a pH greater than 6 is yellow, while the concentration boundary layer, with a pH smaller than 4 is red. The pattern traced by the indicator can be used to analyse the shape and thickness of the concentration boundary layer, and to study the effect of fluid flow on the phenomena taking place in the proximity of the membrane surface in an electrodialysis cell.

4. Results

4.1. *Results obtained from the limiting current density*

To compare the experimental results obtained from the visualization technique proposed in this work, the thickness of the concentration boundary layer was first determined from the limiting current density using Equation 1. The limiting current density was determined from the plot of the resistance of the electrodialysis cell, $U/I(\Omega)$ against the reciprocal of the current, $I^{-1}(A^{-1})$, by the Cowan and Brown method [22]. The limiting current density corresponds to the minimum of this plot.

Figure 3 shows a typical plot of $U/I(\Omega)$ against $I^{-1}(A^{-1})$ for a fluid velocity of $3.68 \times 10^{-3}\,m\,s^{-1}$. From the minimum of this plot, a value of 0.145 A was obtained for the limiting current. Then, applying Equation 1, a value of $\delta = 1.72 \times 10^{-3}$ m was obtained for the thickness of the concentration boundary layer, taking into account the properties of the solution, the transport numbers of chloride ions in the membrane, $\bar{t}_{Cl^-}$, and in the solution, t_{Cl^-}, and the membrane exchange area. This value was further compared with the values obtained from the visualization method.

4.2. *Results obtained from the visualization method*

When the cell operates above the limiting current density, hydroxyl ions are transferred from the cathodic compartment to the anodic compartment, across the anionic membrane, while protons remain on the cathodic compartment. This situation leads to a gradient in the proton concentration, or pH difference, from the membrane surface to the bulk of the solution located in the concentration boundary layer, which causes a change in the colour of the analytical indicator from the concentration boundary layer to the solution.

Figure 4 is a visualization of the concentration boundary layer flow immediately following start-up. Figure 4(a) shows the image displayed directly by the video camera, while Figure 4(b) shows the same image after being treated using the image analysis software Aldus® Photostyler®. In Figure 4(a) and (b), the membrane was situated to the left of the picture, and the fluid flowed from bottom to top. The thin red layer adjacent to the membrane corresponds to the concentration boundary layer, while the solution is yellowish coloured. The concentration boundary layer grows from the bottom to the top, in the flow direction, and its shape and thickness are clearly visible, which corresponds to the development of a laminar boundary layer.

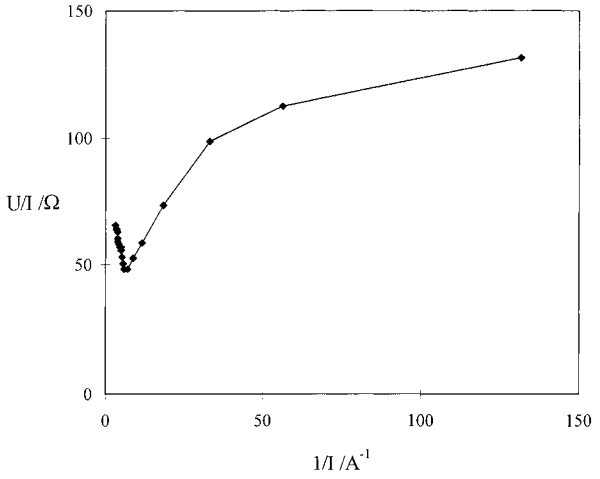

Fig. 3. Determination of the limiting current density. $u = 3.68 \times 10^{-3}\,m\,s^{-1}$.

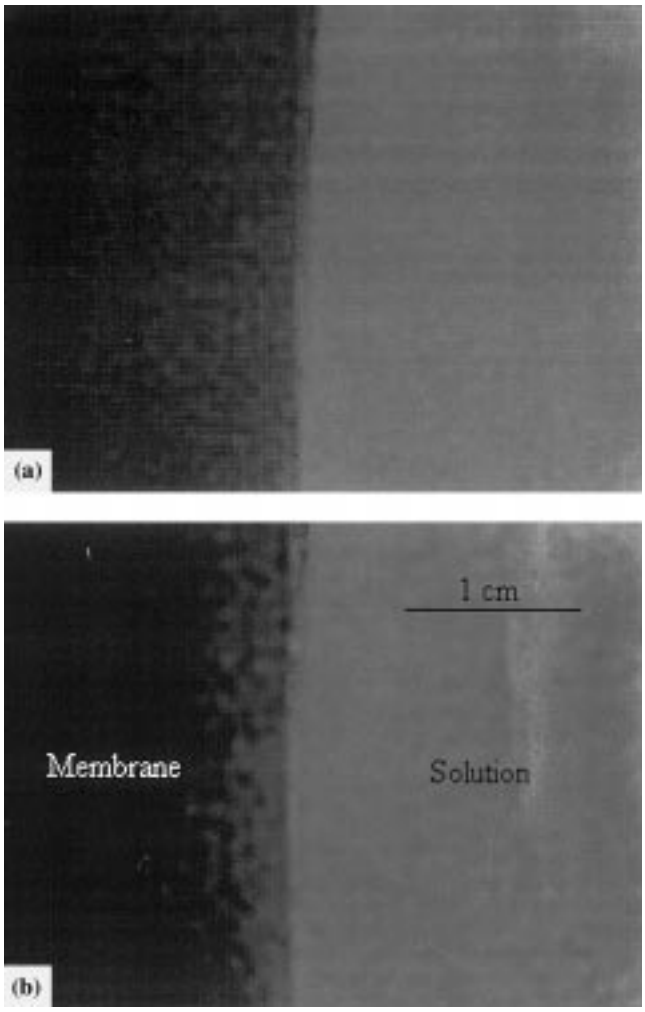

Fig. 4. Visualization of the concentration boundary layer formed on the surface of an anionic membrane. (a) Image obtained directly from the video camera; (b) image after being treated with an image analysis software.

In Figure 5(a–c), photographs of the concentration boundary layer are presented for three different fluid velocities of 7.37×10^{-4}, 2.21×10^{-3} and $3.68 \times 10^{-3}\,m\,s^{-1}$, respectively. As can be seen from the real time photographs, the thickness of the concentration boundary layer decreased when fluid velocity increased, as expected. The thickness of the concentration boundary layer could be determined from the picture by measuring the distance from the membrane surface to the outermost detectable edge. Table 1 shows the values of the thickness of the concentration boundary layer at a

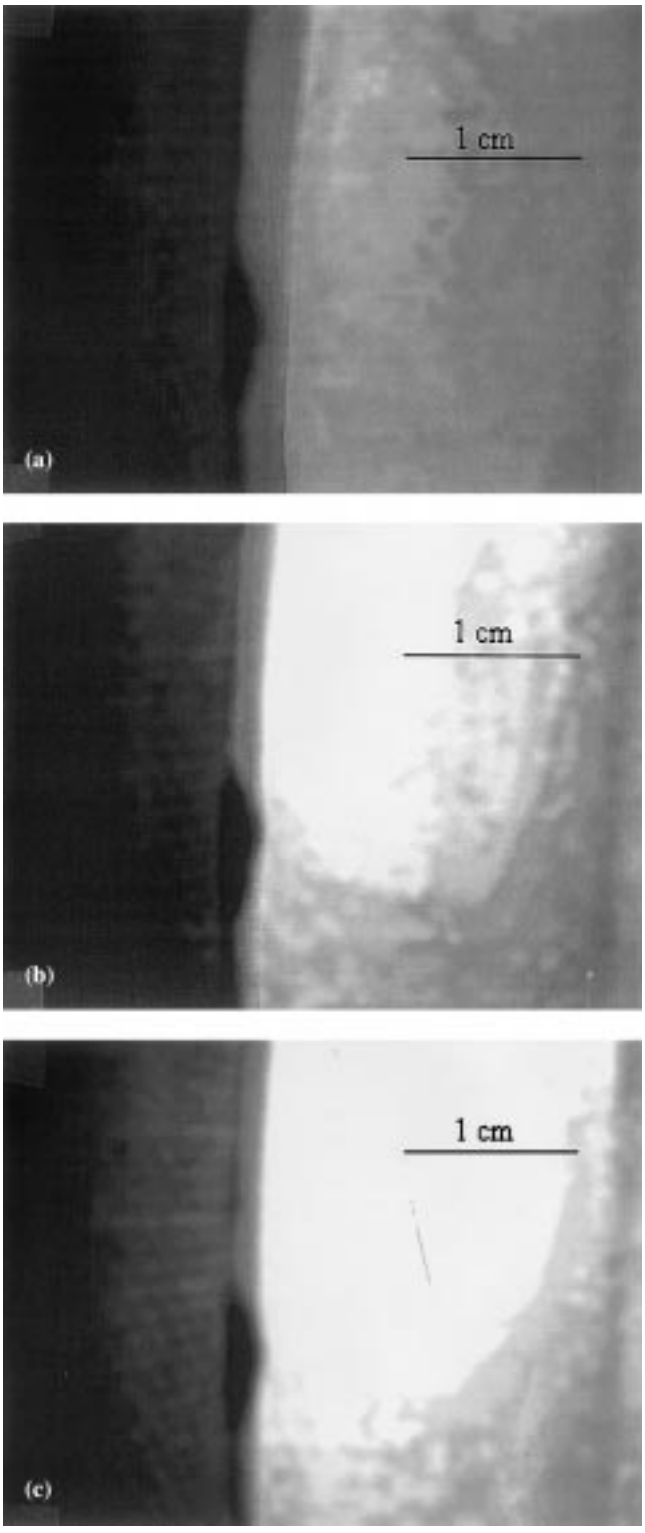

Fig. 5. Concentration boundary layer at different fluid velocities, u: (a) 7.37×10^{-4}, (b) 2.21×10^{-3} and (c) $3.68 \times 10^{-3}\,\mathrm{m\,s^{-1}}$.

distance of 125 mm from the entrance of the fluid to the cell, for each fluid velocity.

The effect of the Reynolds number on the thickness of the concentration boundary layer is shown in Figure 6. The experimental results were compared with values predicted by Equation 2, using the following values for the different parameters: $x = 125\,\mathrm{mm}$ (distance from the entrance of the fluid to the cell at which the concentration boundary layer is measured in the photographs); $x_0 = 100\,\mathrm{mm}$ (distance from the entrance of the fluid to the cell at which the membrane is situated and the concentration boundary layer is formed); and $Sc = 681.45$.

Table 1. Effect of fluid velocity on the thickness of the concentration boundary layer

$u/\mathrm{m\,s^{-1}}$	Re_x	$10^3\,\delta/\mathrm{m}$
7.37×10^{-4}	91.14	3.45
2.21×10^{-3}	273.41	2.18
3.68×10^{-3}	455.69	1.72

As can be seen from Figure 6, good agreement is obtained between the experimental results and the theoretical prediction given by Equation 2. From the least squares fitting of the experimental data obtained from the visualization method, the following correlation between the thickness of the concentration boundary layer and the Reynolds number is obtained:

$$\delta = 3.16\,x\left(\frac{Sc}{X}\right)^{-1/3} Re_x^{-0.43} \tag{4}$$

which is similar to Equation 2.

The values of δ obtained from the visualization method agree well with those obtained from the limiting current density given by Equation 1, as can be concluded from the result indicated in the previous paragraph for a fluid velocity of $3.68 \times 10^{-3}\,\mathrm{m\,s^{-1}}$. Similar results were obtained for other fluid velocities.

Figure 7(a–e) shows a sequence of photographs taken at different times when a pulsation with a frequency, ω of $3\,\mathrm{s^{-1}}$ and an amplitude, a of 8 mm was added to a steady flow of bulk mean velocity, u of $3.68 \times 10^{-3}\,\mathrm{m\,s^{-1}}$, a situation which corresponds to reverse flow. As a

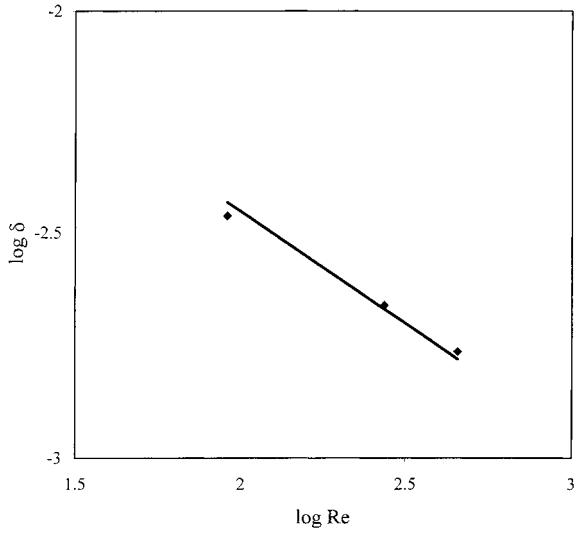

Fig. 6. Effect of Reynolds number on the thickness of the concentration boundary layer. Key: (◆) experimental data; (—) Equation 2.

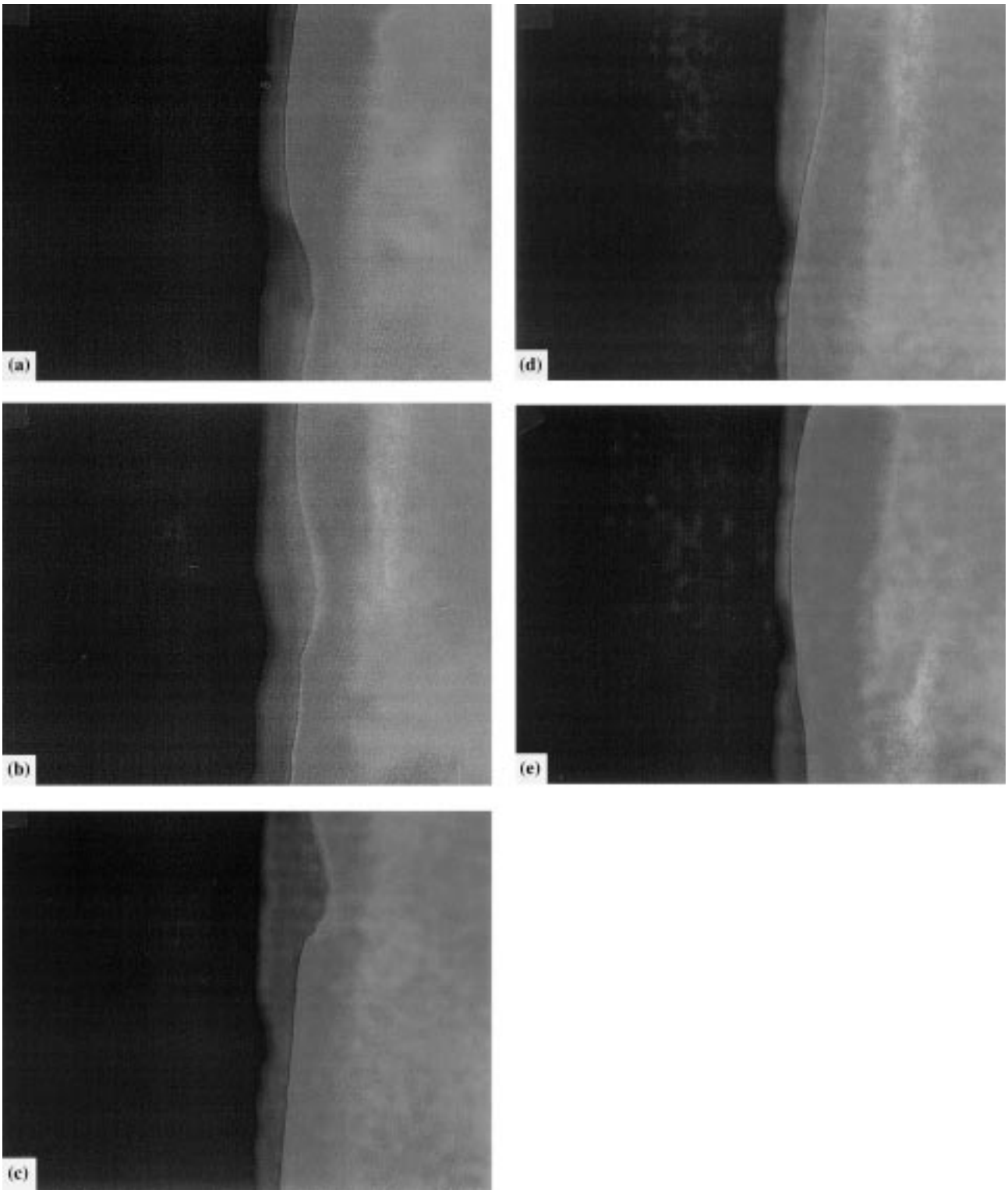

Fig. 7. Effect of pulsating flow on the concentration boundary layer, $\omega = 3.0\,s^{-1}$, $a = 8 \times 10^{-3}\,m$, $u = 3.68 \times 10^{-3}\,m\,s^{-1}$. (a) $t = T/5\,s$, (b) $t = 2T/5\,s$, (c) $t = 3T/5\,s$, (d) $t = 4T/5\,s$ and (e) $t = T\,s$.

consequence of the pulsation, the shape and thickness of the concentration boundary layer change with time, and vortices are developed through a pulsation period due to the instability of the concentration boundary layer caused by the pulsating flow. These vortices move, oscillating in the direction of the main flow, changing its size through a pulsation period as a consequence of the instantaneous change of the velocity profile on the membrane surface due to the induced pulsation. Finally, the vortices disperse into the bulk solution, and then, protons are transferred to the solution. These visualization studies suggest that mass transfer enhancement across an ion exchange membrane in pulsating flow observed in other works [16, 23], may be due to the

periodic renewal of the liquid in the wall boundary layer as can be concluded by the formation of the vortices and their dispersion in the bulk of the solution.

Figure 8(a–c) shows the evolution of the vortices obtained at different times after the pulsation system was switched off. The pattern seen in this case is an integrated effect of the previous oscillatory movement. The flow became unstable, then vortices were formed and separated from the concentration boundary layer, and were transferred to the bulk of the solution as a result of the deceleration caused by stopping the pulsation system.

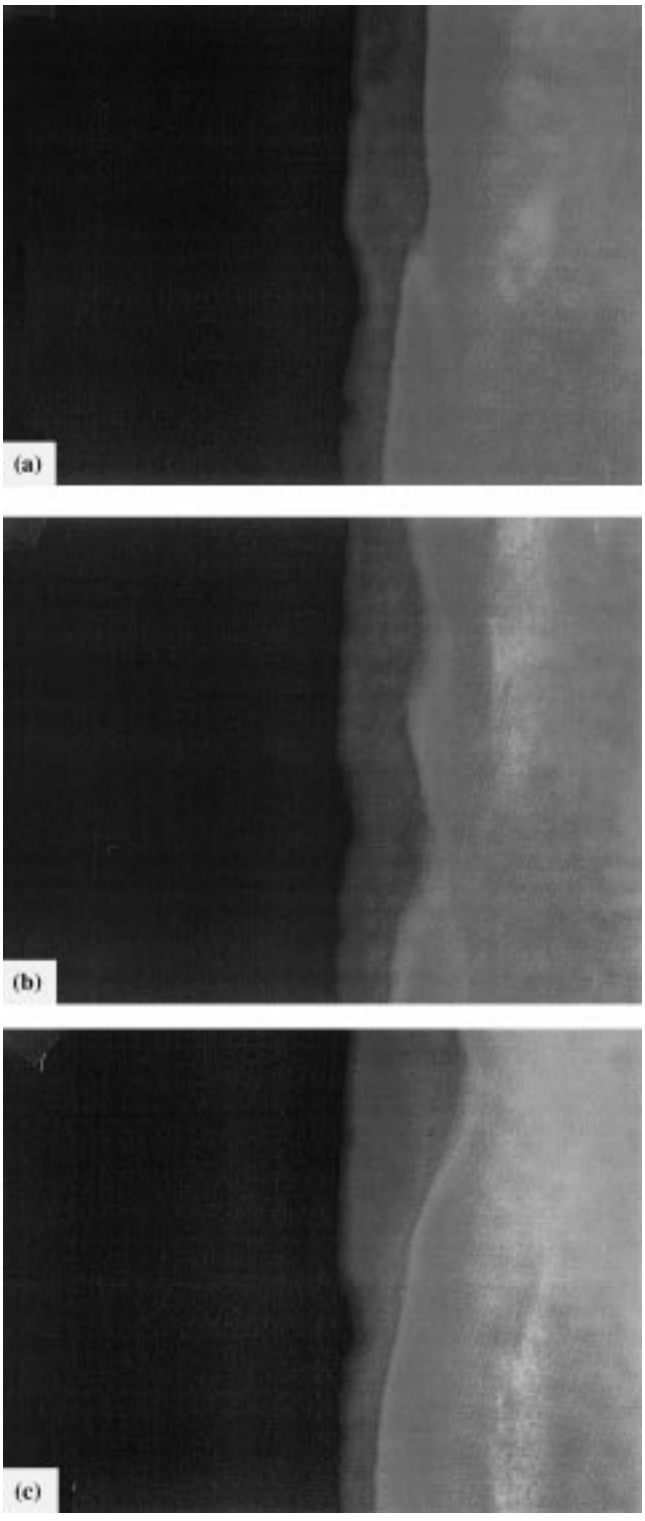

Fig. 8. Visualization of the concentration boundary layer at different times after the pulsation system is stopped. (a) $u = 3.68 \times 10^{-3}\,\mathrm{m\,s^{-1}}$, $t = 0\,\mathrm{s}$, (b) $u = 3.68 \times 10^{-3}\,\mathrm{m\,s^{-1}}$, $t = 5\,\mathrm{s}$ and (c) $u = 3.68 \times 10^{-3}\,\mathrm{m\,s^{-1}}$, $t = 10\,\mathrm{s}$.

5. Conclusions

A new method for the visualization of the concentration boundary layer at the surface of an ion exchange membrane has been proposed. The main advantage of this method is that it does not disturb the flow, as the colour change of the analytical indicator used takes place due to the protons generated on the membrane surface when the limiting current density is exceeded. The formation of the concentration boundary layer and its development along the membrane surface were clearly visualized.

The thickness of the concentration boundary layer decreases as the fluid velocity increases. In general, a good agreement between experimental and theoretical results is obtained under laminar boundary layer conditions. Measurement of the thickness of the concentration boundary layer using the visualization technique agrees well with data obtained from other techniques such as limiting current density measurement.

In pulsating flow the thickness and shape of the concentration boundary layer change with time during the pulsation period. Vortices are formed and transferred to the bulk solution. This situation contributes to the periodic renewal of the concentration boundary layer and leads to mass transfer enhancement across the membrane.

References

1. W. Merzkirch, 'Flow Visualization II', Proceedings of the Second International Symposium on Flow Visualization (McGraw-Hill International, Bochum, West Germany, 1980).
2. Y. Nakayama, W.A. Woods and D.G. Clark, 'Visualized Flow' (The Japan Society of Mechanical Engineers. Pergamon Press, Oxford, 1988).
3. S.M. Tieng and Y.C. Wang, *J. Fluids Eng.* **115** (1993) 515.
4. T. Sarpkaya, *J. Fluid Mech.* **253** (1993) 105.
5. S. Kato and N. Maruyama, *JSME International J.* **37** (1994) 912.
6. W. Schöpf and J.C. Patterson, *J. Fluid Mech.* **295** (1995) 357.
7. H.I. Abu-Mulawek, B.F. Armaly and T.S. Chen, *J. Heat Transfer* **117** (1995) 895.
8. J.P. Johnston and K.A. Flack, *J. Fluids Eng.* **118** (1996) 219.
9. V. Sanchez and M. Clifton, *J. Chim. Phys.* **77** (1980) 421.
10. V.A. Shaposhnik, O.V. Grigorchuk, E.N. Korzhov, V.I. Vasil′eva and Y. Ya Klinov, *J. Mem. Sci.* **139** (1988) 85.
11. M. Taky, G. Pourcelly, F. Lebon and C. Gavach, *J. Electroanal. Chem.* **336** (1992) 171.
12. G. Saracco, M.C. Zanetti and M. Onofrio, *Ind. Eng. Chem. Res.* **32** (1993) 657.
13. M. Law, T. Wen and G.S. Solt, *Desalination* **109** (1997) 95.
14. P. Sistat and G. Pourcelly, *J. Mem. Sci.* **123** (1997) 121.

15. R.C. Weast, 'Handbook of Chemistry and Physics', 70th edn (CRC Press, Boca Raton, FA, 1990).
16. V. Pérez-Herranz, J.L. Guiñón and J. García-Antón, *J. Appl. Electrochem.* **27** (1997) 469.
17. B.A. Cooke, *Electrochim. Acta* **3** (1961) 307.
18. Y. Tanaka, M. Iwahashi and M. Kogure, *J. Mem. Sci.* **92** (1994) 217.
19. E. Costa, 'Fenómenos de Transporte' (Alhambra. Madrid, 1984).
20. C. Bengoa, A. Montillet, P. Legentilhomme and J. Legrand, *J. Appl. Electrochem.* **27** (1997) 1313.
21. J.H. Gerard, *J. Fluid Mech.* **46** (1971) 43.
22. D.A. Cowan and J.H. Brown, *Ind. Eng. Chem.* **51** (1959) 1445.
23. V. Pérez-Herranz, J. García-Antón and J.L. Guiñón, *Chem. Engng. Sci.* **52** (1997) 843.